Frequency band broadening and charge density enhancement of a vibrational triboelectric nanogenerator with two stoppers

Qi, Youchao; Liu, Guoxu; Kuang, Yang; Wang, Lu; Zeng, Jianhua; Lin, Yuan

DOI:
10.1016/j.nanoen.2022.107427

Publication date:
2022

Nano Energy 99 (2022) 107427

Contents lists available at ScienceDirect

Nano Energy

journal homepage: www.elsevier.com/locate/nanoen

Frequency band broadening and charge density enhancement of a vibrational triboelectric nanogenerator with two stoppers

Youchao Qi [a,c,1], Guoxu Liu [a,c,1], Yang Kuang [b,1], Lu Wang [d], Jianhua Zeng [e], Yuan Lin [e], Han Zhou [e], Meiling Zhu [b,*], Chi Zhang [a,c,e,**]

[a] CAS Center for Excellence in Nanoscience, Beijing Key Laboratory of Micro-nano Energy and Sensor, Beijing Institute of Nanoenergy and Nanosystems, Chinese Academy of Sciences, Beijing 101400, China
[b] College of Engineering, Mathematics and Physical Sciences, University of Exeter, Exeter EX4 4QF, UK
[c] School of Nanoscience and Technology, University of Chinese Academy of Sciences, Beijing 100049, China
[d] State Key Laboratory for Manufacturing Systems Engineering, International Joint Laboratory for Micro/Nano Manufacturing and Measurement Technologies, Collaborative Innovation Center of Suzhou Nano Science and Technology, Xi'an Jiaotong University, Xi'an 710049, China
[e] Center on Nanoenergy Research, School of Physical Science and Technology, Guangxi University, China

ARTICLE INFO

Keywords:
Triboelectric nanogenerator
Charge pump
Nonlinear impact force
Wideband vibration
Surface charge density

ABSTRACT

Vibrational triboelectric nanogenerators (V-TENG) can be used to harvest broadband vibration energy due to the nonlinear impact force induced by a stopper. However, V-TENGs with a single stopper have limited bandwidth and surface charge density, which has limited their application in wideband vibration energy harvesting. Herein, a V-TENG with two stoppers and a charge pumping effect is proposed for frequency band broadening and charge density enhancement. The theoretical analysis and experimental validation have indicated the V-TENG with two stoppers could improve the bandwidth by 75% compared with one stopper at a gap distance of 0.5 mm. Moreover, a charge pump can be constructed with two output channels, which has improved surface charge density by about 14 times. With the frequency varying from 18 to 38 Hz, the V-TENG can continually power 400 LEDs and charge a commercial capacitor quickly. This work has shown an encouraging method for enhancing the performance of V-TENGs, which also has great prospects in harvesting wideband vibration energy from machines, cars, ships, and human motions for self-powered electronics.

1. Introduction

With the rapid development of wireless sensor networks [1–3], environmental energy harvesting is expected to become the main energy source, which can replace the traditional power supply by battery or wire [4–6]. Vibration energy is the most widely distributed in the environment and can be found in mechanical equipment, building structures, water waves, breeze blowing, and our daily activities [7,8]. Three conventional transduction mechanisms including electrostatic [9,10], electromagnetic [11], and piezoelectric [12] can convert ambient vibrational energy into useful electric power. Here, an urgent challenge in vibrational energy harvesting is to enhance the performance under a wide working bandwidth. This is because traditional vibration energy harvesters can only work in a narrow frequency range [13], which severely limits its practical application for random and broadband vibration. As a result, various strategies such as multi-modal [14,15], and nonlinear technologies [16–18] have been proposed to overcome this issue to achieve wideband energy harvesting. However, the multi-modal method usually requires the integration of multiple units, which limits its development for harvesting wideband vibration energy. In contrast, the nonlinear ways only need to add the stoppers to harvest wideband vibration energy without increasing design size, which is significant for wideband energy harvesting.

Triboelectric nanogenerators (TENG) proposed by Wang [19] in 2012 present superiorities including high efficiency [20,21], wide material selection [22,23], easy fabrication [24,25],lightweight [26,27], as well as unique features based on the contact electrification effect and electrostatic induction [28,29]. Thereof, vibrational TENGs (V-TENG)

* Correspondence to: College of Engineering, Mathematics and Physical Sciences, University of Exeter, UK.
** Correspondence to: Tribotronics Research Group, Beijing Institute of Nanoenergy and Nanosystems, Chinese Academy of Sciences, China.
E-mail addresses: m.zhu@exeter.ac.uk (M. Zhu), czhang@binn.cas.cn (C. Zhang).
[1] These authors contributed equally to this work.

https://doi.org/10.1016/j.nanoen.2022.107427
Received 12 April 2022; Received in revised form 7 May 2022; Accepted 22 May 2022
Available online 25 May 2022

produce energy through repeated contact and separation, which the energy generation mechanism will cause a nonlinear feature and harvest broadband vibration energy. However, some research has focused on a single V-TENG with one stopper [30–32], which has limited bandwidth. In addition, a low surface charge density [33] produced by the V-TENG greatly reduces their power output in wideband vibration energy harvesting. Up to now, the methods to overcome the problem mainly focus on ionized-air injection [34], environment control [35], structure optimization [25], and the selection of materials [23]. The surface charge density increases to some extent by these methods, but the charges are static and cannot realize a long-time operation. As a result, it's important to develop advanced mechanisms and methods like the charge pump [36] for achieving wideband energy harvesting of the V-TENG with high surface charges.

Here, a V-TENG based on two stoppers is demonstrated for frequency band broadening and charge density enhancement. The frequency band broadening is achieved by double-sided stoppers and the charge density enhancement is realized by the charge pump. The theoretical analysis and experimental validation with different excitation accelerations and initial gap distances have indicated a broader bandwidth with two stoppers by about 75% than that with one stopper under the gap distance of 0.5 mm. In addition, the V-TENG based on a charge pump (CPV-TENG) with a high output performance is constructed according to the two output channels of the V-TENG, which can obtain a high surface charge density and has improved by about 14 times. With the charge pump, the V-TNEG can continually power 400 LEDs and charge a commercial capacitor quickly under a broadband frequency change from 18 to 38 Hz. In addition, V-TENG can quickly drive a temperature sensor and a pressure sensor to work. This work delivers to essential strategy for developing a high-performance V-TENG, which would be meaningful for building the self-powered intelligent sensor networks and developing the energy internet.

2. Results and discussion

2.1. Structure and working mechanism of the V-TENG

The V-TENG with two stoppers and its working process based on contact and separation mode are shown in Fig. 1. The fixed part, the moving assembly composed of a top moving part and a bottom moving part, and the springs establish the main structure of the V-TENG, while the moving assembly and the fixed part produce electrical output by repeated contact and separation. As shown in Fig. 1a, the fixed part consists of two triboelectric films (Kapton and Polytetrafluoroethylene (PTFE)), which were selected because of their high dielectric constants and excellent contact electrification properties, respectively. Furthermore, a layer of sponge is attached to one side of each triboelectric film and connected to the acrylic substrate introducing contact stiffness k_1 and k_2. The surface of the PTFE was modified by sandpapers (10,000 grit) to enhance the contact area between the two friction films (PTFE and Cu) and improve electric output. Fig. 1a shows the surface topography of the enhanced PTFE, obtained by scanning electron microscopy (SEM). Each moving part consists of a copper film as the triboelectric layer, which was opted for due to its good conductivity and contact

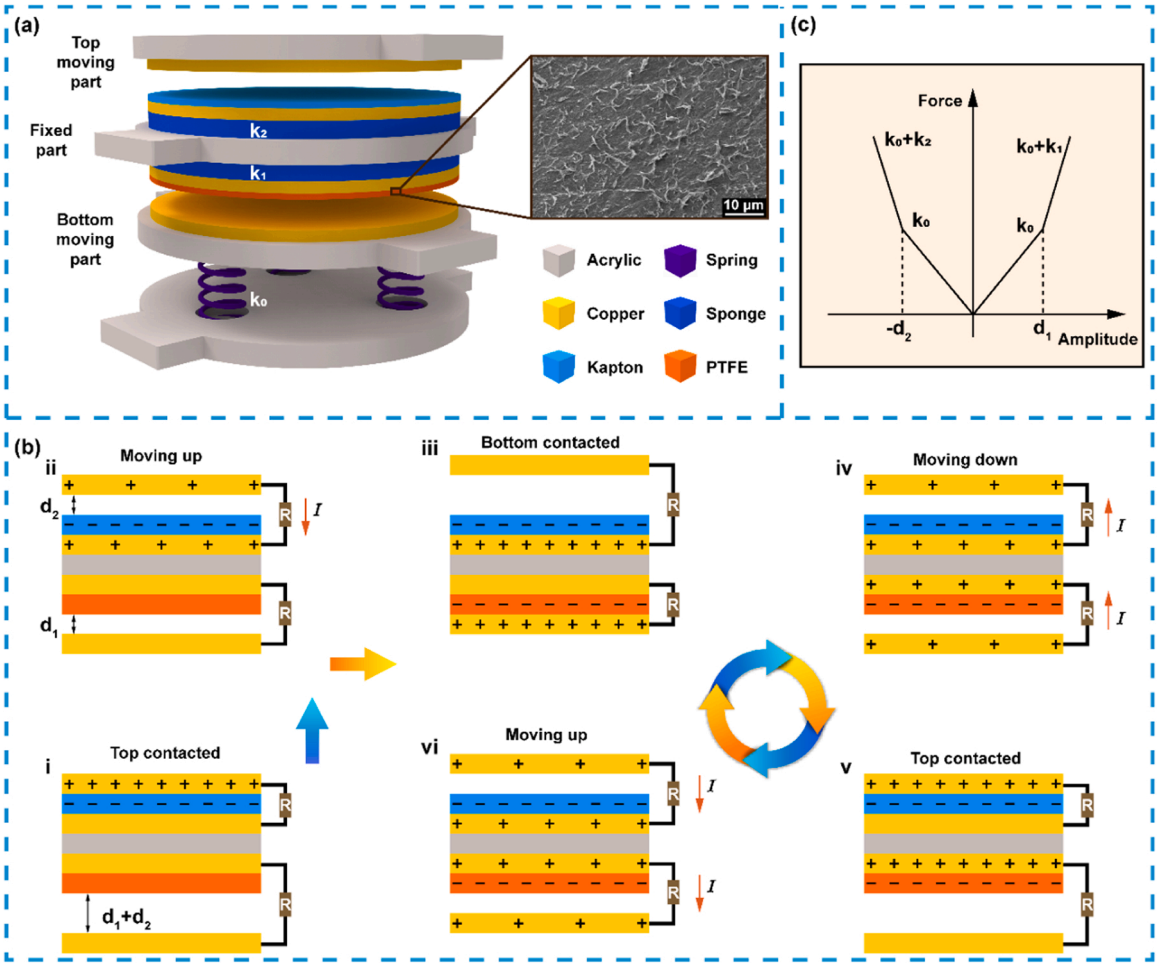

Fig. 1. Device demonstration and working process of the vibrational triboelectric nanogenerator (V-TENG). (a) The whole structure of V-TENG with an inset of micro-nanostructures. (b) Working process of the V-TENG under vibration conditions. (c) The stiffness changes of V-TENG under different vibration amplitudes.

electrification properties. The springs are used to store and release elastic forces and have inherent stiffness k_0. Acrylic is used as the supporting component owing to its high stability and good processability. The fabrication process of the V-TENG with two stoppers is discussed in the Experimental Section in detail.

Fig. 1b (i-vi) shows the working process of the V-TENG with two stoppers based on the contact separation mode. Assuming that the moving assembly moves downwards firstly when an external excitation acts on the V-TENG, the top moving part will contact the Kapton triboelectric layer, and the bottom moving part and the PTFE friction layer will arrive at a maximum distance (d_1+d_2), as shown in Fig. 1b (i). In the meantime, the copper friction layer and the Kapton friction layer will obtain equal positive and negative charges, respectively. Then, the top moving part begins to leave the Kapton friction layer (Fig. 1b (ii)), and the negative charges will transfer from the Kapton electrode layer to the copper film due to the function of electrostatic potential. With the continuous external excitation, the two triboelectric films are separated to the maximum distance (Fig. 1b (iii)). Meanwhile, the bottom moving part will contact the PTFE triboelectric layer and the PTFE film will obtain electrons from the copper film while the copper film acquires the same number of positive charges. Then, the bottom moving part will move down and reach the maximum distance on account of the continuous excitation vibration (Fig. 1b (iv-v)). During this process, the negative charges will transfer from the PTFE electrode layer and the copper film of the top moving part to the copper film of the bottom moving part and the Kapton electrode layer, respectively, due to the function of electrostatic potential. After the bottom moving part begins to move upwards (Fig. 1b (vi)), the electrons will move in the opposite direction under the function of electrostatic potential. This is the whole charge transfer process for one vibrational cycle of the V-TENG. It is worth noting here that the top moving part and the bottom moving part can be considered as two stoppers. During the working process of the V-TENG, the two stoppers will cause the V-TENG explicit a nonlinear feature. Fig. 1c illustrates a piecewise linear model of the V-TENG with two stoppers. When the bottom moving part contacted the fixed part, the overall stiffness of the system was increased from k_0 to k_0+ k_1. When the top moving part contacted the fixed part, the overall stiffness of the system was then increased from k_0 to k_0+ k_2. As a result, the V-TENG with two stoppers will have a broader frequency band.

2.2. The mechanical model and simulated frequency band characteristic

The V-TENG was modelled as a single-degree-of-freedom system with piecewise linear stiffness [13] to investigate its characteristics of frequency band broadening (Fig. 2a). The moving assembly is represented as a mass-spring-damper system with mass block m, a spring stiffness k_0, and a damping factor c_0. Each side of the fixed part is modelled by as a spring with the stiffness of k_1 (k_2) and a damper with a coefficient of c_1 (c_2). The initial distance between the fixed part and the top (bottom) moving part is d_2 (d_1). The motion of the base is defined as y and the motion of the moving assembly relative to the base is defined as z. The relative motion of the moving assembly can be considered with three cases. In the first case, the motion of the moving assembly is within the set distances of d_1 (assume d_1 is less than d_2), and the whole system has a stiffness and damping coefficient of k_0 and c_0, respectively. In the second case, the moving assembly moves upward and surpasses the distance d_1. As a result, the whole system has a stiffness and damping coefficient of k_0+ k_1 and c_0+c_1, respectively. In the third case, the moving assembly moves downwards and suppresses the distance d_2, and the whole system has a stiffness and damping coefficient of k_0+ k_2 and c_0+c_2, respectively. The variation of the stiffness with displacement makes the system exhibit nonlinear characteristics. The dynamics of the system can be expressed by Eqs. (1–3).

$$m\ddot{z} + (c_0 + c_1)\dot{z} + k_0 z + k_1(z - d) = -m\ddot{y}, (z \geq d_1) \quad (1)$$

$$m\ddot{z} + c_0\dot{z} + k_0 z = -m\ddot{y}, (-d_2 < z < d_1) \quad (2)$$

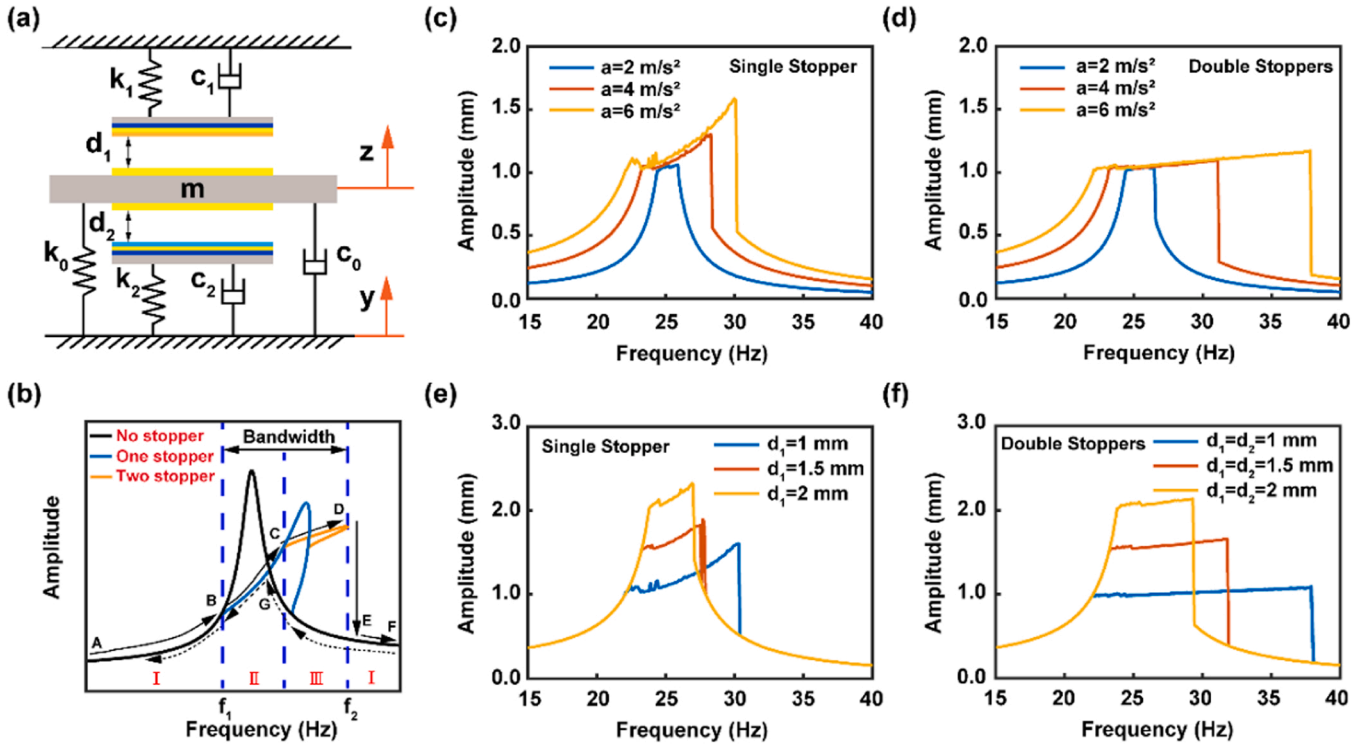

Fig. 2. The mechanical model of single-degree-of-freedom with stoppers on two sides and amplitude response with different parameter conditions of the V-TENG. (a) The mechanical model of single-degree-of-freedom of V-TENG with two stoppers and nonlinear feature parameters. (b) The amplitude response of the V-TENG with a variation of frequency. The amplitude response curve of V-TENG with stoppers on one or two sides when the change of acceleration (c, d), and distance between the fixed parts and moving parts (e, f).

$$m\ddot{z} + (c_0 + c_2)\dot{z} + k_0 z - k_2(z + d) = -m\ddot{y}, (z \leq -d_2) \quad (3)$$

Eqs. (1–3) can be solved by the average method, as demonstrated in the Supporting Information. It should be pointed out that the voltage response of V-TENG is not proportional to the displacement according to Paschen's Law. Furthermore, compared with the elastic force of the spring, the electrostatic force is very small. Therefore, the influence of the electrostatic force is not considered in the model establishment process. Eqs. (1–3) were solved using the commercial software Matlab to obtain the displacement response of the V-TENG during an up-sweeping frequency, as shown in Fig. 2b. In the first part (I), the motion of the V-TENG is below a preset distance of d_1 and the two sides of the fixed part are not in contact with the stopper. As a result, the motion of the V-TENG follows the linear model and varies monotonically from point A to point B with up-sweeping frequency. At point B, the bottom moving part is in contact with the fixed part. As a result, the motion of the V-TENG becomes a piecewise linear model with one stopper in the second part (II). Then, the motion amplitude augments from point B until it contacts the top moving part at point C. Hence, the motion of the V-TENG becomes a piecewise linear model with two stoppers in the third part (III). Then, the amplitude of the V-TENG would continuously vary from point C to point D. Therefore, the bandwidth of V-TENG with two stoppers is wider than one stopper, which can arrive at (f_2-f_1). At point D, the motion of the V-TENG drops immediately to point E. The reason is that there will be multiple amplitude solutions in the nonlinear interval. And the motion amplitude varies steadily along with the maximum value only during the up-sweeping frequency, and linearly thereafter. Finally, the motion of the V-TENG reverts to the linear model in the first part (I) and varies monotonically from point E to point F. This is the variation law of the amplitude of V-TENG with up-sweeping frequency. In contrast, the amplitude of V-TENG would change from point F to point A along the dotted line with the down-sweeping frequency, and the frequency band would not be extended.

The amplitude change law of the V-TENG under different initial distances and excitation accelerations was simulated (Fig. 2(c-f)). And Fig. S1 showed the schematic diagram of the structure of the V-TENG with one stopper and its mechanical model. Therein, Figs. 2c and 2d showed the amplitude change law of V-TENG with one stopper and two stoppers at different accelerations. Here, the initial distances of the V-TENG with one and two stoppers were all set to 1 mm. The mass m was set as 120 g, and the stiffness k_0, k_1, and k_2 were set as 1.5×10^2, 1×10^5, and 1×10^{12} N/m, respectively in the simulation. It can be seen that the V-TENG would obtain a larger working frequency range with the increase of acceleration from 2 to 6 m/s^2. What's more, the frequency response of the V-TENG with two stoppers was wider than the one stopper, which is mainly reflected in the third part. Figs. 2e and 2f showed the amplitude change law of V-TENG with one stopper and two stoppers at different initial distances. Here, the accelerations of the V-TENG with one and two stoppers were all set to 6 m/s^2. And the mass and stiffness remain unchanged in the simulation. It can be concluded that the V-TENG would obtain a narrower working frequency range with the increase of distance from 1 to 2 mm. Simulation results suggest that the acceleration and the initial distance have significant influences on the working bandwidth of the V-TENG with both one stopper and two stoppers.

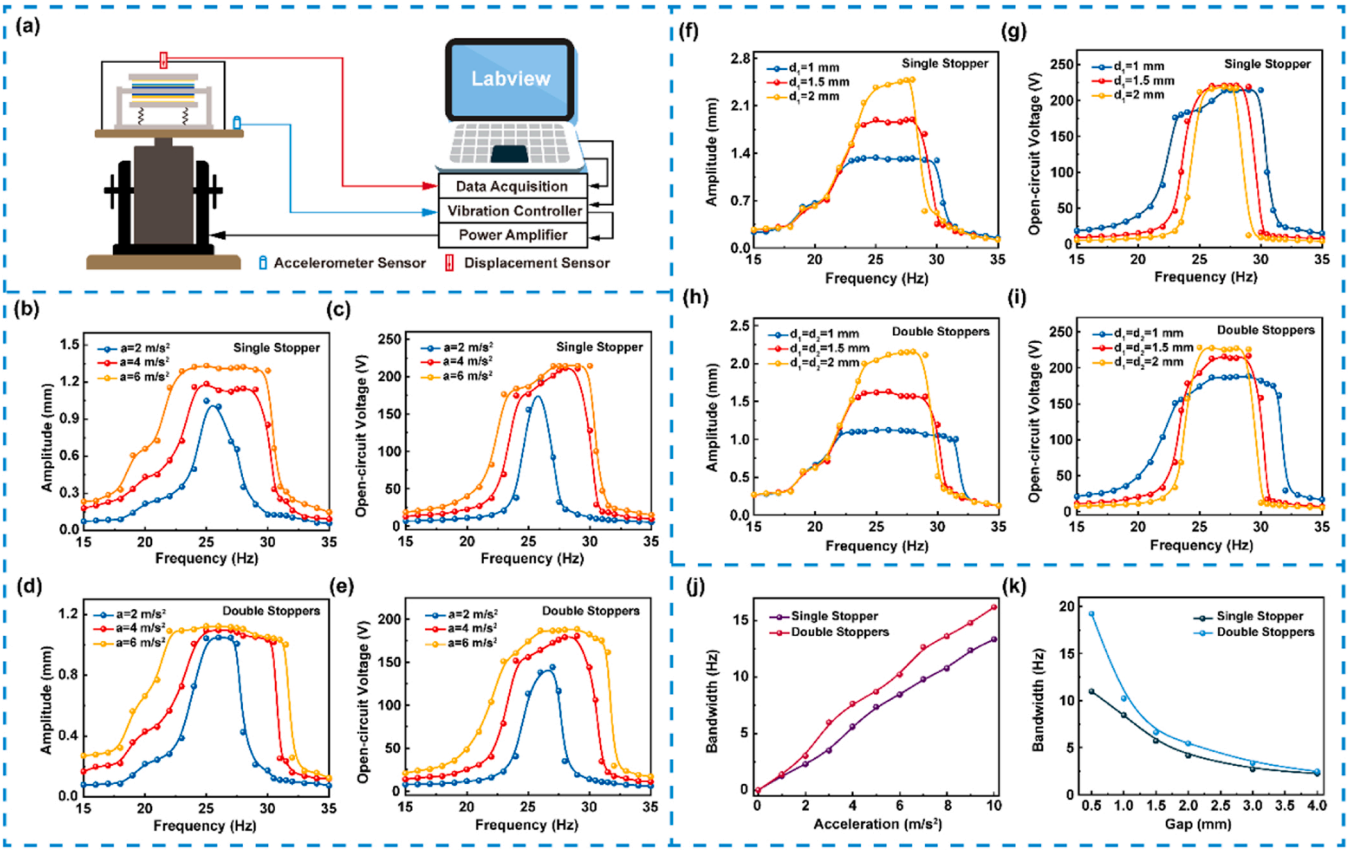

Fig. 3. Amplitude frequency response and voltage characteristic, and bandwidth change rule at different parameter conditions. (a) The test setup for measuring the amplitude and voltage response of the V-TENG. The change rule of amplitude (b, d), output voltage (c, e), and bandwidth (j) under different base accelerations of V-TENG with stoppers on one or two sides. The change rule of amplitude (f, h), output voltage (g, i), and bandwidth (k) under a different initial distance between the fixed parts and moving parts of V-TENG with stoppers on one or two sides.

2.3. Experimental validation for the displacement and voltage response of V-TENG

An experiment platform (Fig. 3a) was built to measure the displacement response and electrical output of the V-TENG. The platform includes an acceleration sensor, a displacement sensor, a vibration control system, and a data acquisition system. The effects of key parameters including acceleration a, distance d_1 or d_2, and stopper number were tested, as shown in Fig. 3(b-k). Here, it should be noted that the two triboelectric layers will come into contact and produce electrical output if the displacement of the V-TENG is larger than d_1 or d_2. When the displacement is less than d_1 or d_2, the triboelectric layers will not contact and the electrical output will be small due to there being no contact electrification process. Consequently, the trend of the voltage response is similar to that of the amplitude-frequency characteristic curve. From Figs. 3b to 3e, it can be observed that the frequency band of V-TENG with both one and two stoppers becomes larger as the acceleration is increased from 2 to 6 m/s^2. However, the measured frequency band is smaller than the simulated. The possible reason is that the actual test process is not ideal, and there will be some external interference, such as the damping will change, and the electrostatic force will also have some interference in the actual test. But the change rule and the simulation results are the same. By comparing the amplitude and voltage response of V-TENG with one and two stoppers, the working bandwidth of V-TENG with two stoppers had been broadened than one stopper. In Fig. 3h, the frequency band of V-TENG with two stoppers became smaller as the distance changed from 1 mm to 2 mm. Meanwhile, the voltage response of V-TENG showed that the frequency band would be smaller due to the distance increasing (Fig. 3i). The experimental outcomes of V-TENG with one stopper demonstrated the same change rules, as shown in Fig. 3f and 3g. By comparing Fig. 3g and 3i, the voltage output of the V-TENG was lower when the distance was 1 mm. This may be because the gap distance was small and the two triboelectric layers were not in close contact. The output can be improved by replacing the sponge with a softer one to bring the two frictional electric layers into closer contact. But, all of these experimental test results and the simulation results are the same. What's more, the frequency band of V-TENG with two stoppers also had been broadened than the V-TENG with one stopper under different gap distances. By analyzing the above experimental and simulation results, the V-TENG with two stoppers will have a wider working bandwidth as an appropriate acceleration and distance. Therefore, the effect of acceleration and distance on working bandwidth had been deeply researched and concluded, as shown in Figs. 3j and3k. And Fig. S2 further showed the change rule of the bandwidth of V-TENG when the acceleration exceeds 10 m/s^2. In addition, when the initial distances set by d_1 and d_2 were different, the frequency band change rules of the V-TENG were also explored through experiments, as shown in Fig. S3. The change rule of the frequency band of the V-TENG with different initial distances d_1 and d_2 is consistent with the V-TENG with the same initial distances d_1 and d_2. Consequently, by decreasing the

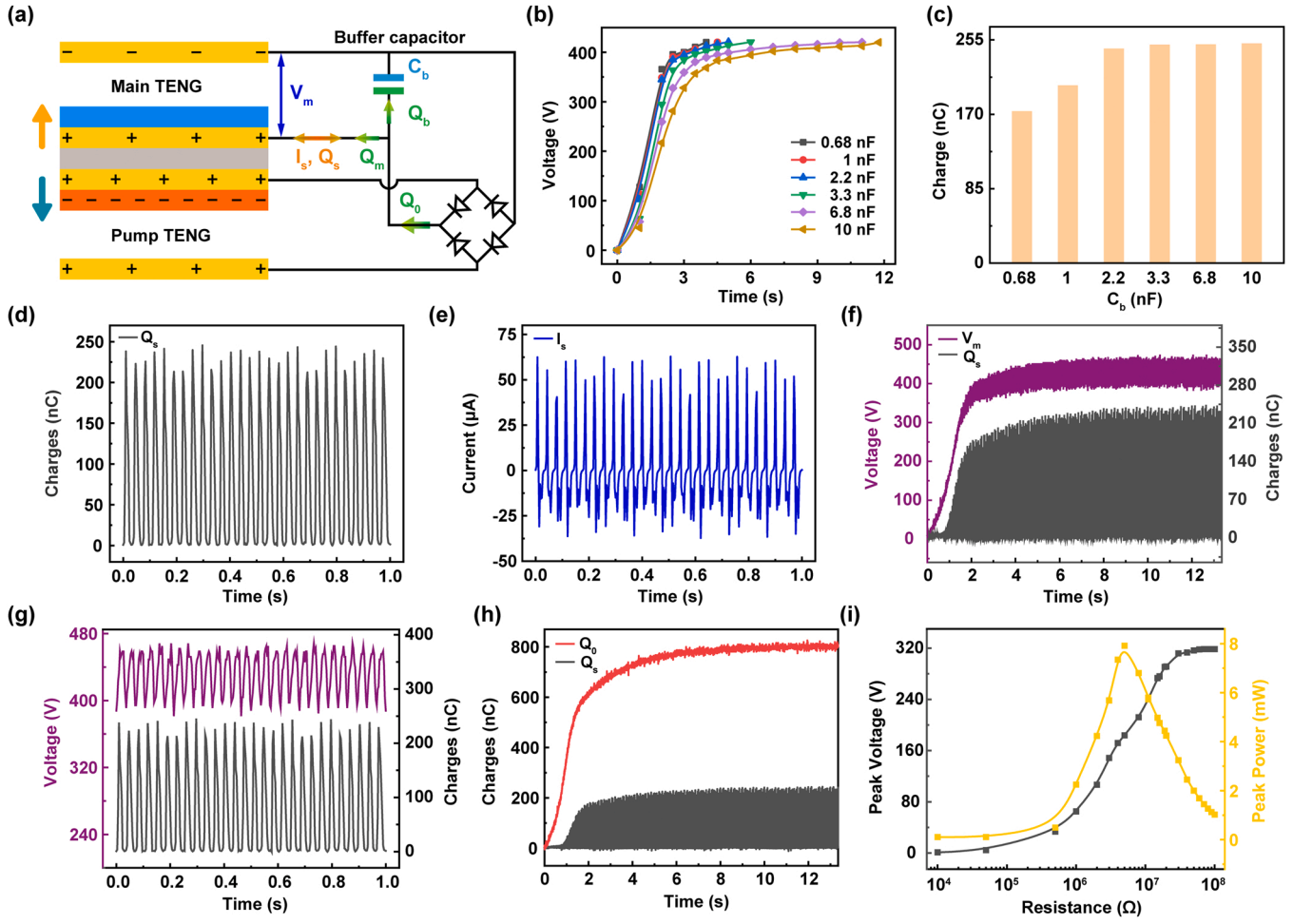

Fig. 4. The output performance characterization of CPV-TENG. (a) The composition of CPV-TENG is based on the dual output channels of V-TENG. (b) The voltage response of the CPV-TENG with various capacitors. (c) With different capacitors, the saturation charge of the CPV-TENG can be measured. The charges (d) and current (e) of the CPV-TENG. (f) Transferred charges and voltage of the CPV-TENG with the influence of the pump TENG. (g) Detailed charge and voltage curve of the CPV-TENG. (h) The transferred charges and injected charges of the CPV-TENG. (i) The peak power and voltage of the CPV-TENG under various impedances.

initial distance, spring stiffness, and increasing acceleration there will be a wider working bandwidth of the V-TENG. What's more, decreasing the spring stiffness can make the working frequency of the V-TENG lower frequency. As a result, by choosing appropriate initial distance, acceleration, and spring stiffness, the V-TENG can be designed to have a wider working bandwidth to harvest broadband vibration energy.

2.4. The output characteristics of V-TENG based on the charge pump (CPV-TENG)

Having analyzed the characteristics of the V-TENG with two stoppers for frequency band broadening, the output characteristics of V-TENG based on the charge pump (CPV-TENG) are further characterized. Fig. 4a showed the basic composition of the CPV-TENG, which consisted mainly of the main TENG, a pump TENG, and a commercial capacitor. The two output channels of the V-TENG can form the main TENG and a pump TENG, while the commercial capacitor was used to buffer charge (referred as buffer capacitor). The working process of the CPV-TENG was demonstrated in Fig. S5. And the charge can be transferred between the main TENG and the buffer capacitor due to the change in the capacitance of the main TENG. Fig. S4 showed the charge density of the CPV-TENG. By gathering charges on both sides simultaneously, the elevated total effective surface charge density could arrive at 251 μC m^{-2}, which increases the surface charge density by about 14 times. Fig. S6 showed the output response of the main and pump TENG to further explore the output features of the CPV-TENG. When there is no pump TENG to inject charge, the charge density can only arrive at 18 μC m^{-2} for the main TENG. When the pump TENG continuously injects charge into the main TENG, the voltage of the main TENG (V_m), transferred charges (Q_s), short-circuit current (I_s), and the injected charges (Q_0) were measured. And the test method is provided in Fig. S7. With different buffer capacitors, the charge saturation curves of the main TENG under the excitation frequency of 28 Hz and the excitation acceleration of 8 m/s^2 were shown in Fig. 4b, which demonstrated a larger capacitance would result in slower charging. Fig. 4c further showed the amount of transferred charges that can be obtained under different buffer capacitors. As the buffer capacitor increased from 0.68 to 10 nF, the transferred charges also augmented and arrived at the stable. This may be due to the inability of small capacitors to store more charge. Considering that a larger capacitor increases the charging time, the best choice of buffer capacitor should be 2.2 nF.

To measure any more the output response of the CPV-TENG, the above parameters were studied in detail. The electrical charge of the CPV-TENG could arrive at 244 nC (Fig. 4d), and the short-circuit current over 60 μA (Fig. 4e) under the excitation frequency of 28 Hz and excitation acceleration of 8 m/s^2. With the optimized capacitor of 2.2 nF, the Q_0, Q_s, and V_m of the main TENG were measured, as shown in Fig. 4(f-h). The Q_s and V_m became larger from zero to arrive at a stable condition with the augment of Q_0. During this process, only a fraction of Q_0 was transferred between the capacitor and the main TENG, while the rest was stored in the capacitor. This may be caused by the insufficient capacitance change of the main TENG. Within 8 s, the voltage continued to rise and reached a high level of about 420 V. Then, the voltage remained stable, and no more charge was injected afterward. At the moment, the injected charges were about 800 nC, the maximum transferred charges were approximately 244 nC. There was no longer a charge transferred between the main TENG and the buffer capacitor. The reason for the small change in the capacitance of the main TENG may be because of the insufficient contact separation caused by the unstable vibration condition of the main TENG. Then, the long-term stability of the CPV-TENG was tested (Fig. S8), and after 50000 cycles, its output performance is almost unchanged. In addition, the power response of the CPV-TENG at various impedances was also measured in detail. The peak power and average power of the CPV-TENG can arrive at 7.8 mW and 520 μW at a resistance of 5 MΩ (Fig. 4i and Fig. S9), respectively.

2.5. The performance and application of CPV-TENG as a power source

Such a high-performance CPV-TENG with wide working bandwidth has extensive application prospects in many areas like vibration energy harvesting for machines, ships, cars, and human activities as shown schematically in Fig. 5a. Located in the machine equipment and human motions, the CPV-TENG can be used to drive different movable electronics like smartphones, smartwatches, thermometer sensors, etc. Furthermore, the output response of the CPV-TENG was measured and recorded under a wide vibration excitation condition. Fig. 5b showed the frequency band characteristics of the CPV-TENG, which can continually obtain a broadband and high charge output from 18 to 38 Hz. As a visual demonstration of outstanding performance, the CPV-TENG can easily power 400 LEDs, while the main TENG can only power 25 LEDs without the pump TENG (Video S1 and Fig. 5 g). To additional verify the high output response of the CPV-TENG under wideband conditions, a test circuit (Fig. 5c) was built to quantitatively characterize its output performance. Under the same wide frequency range, the CPV-TENG can perpetually charge the commercial capacitor quickly (Fig. 5d). The detailed charging curve for each frequency was given in Fig. S10. Fig. 5(e, f, h, i) showed the CPV-TENG could be used to drive the temperature and pressure sensors. The pressure sensor can accurately sense the change of external pressure under the drive of the CPV-TENG (Fig. 5(e, h)). And the pressure sensor can work effectively within 18–38 Hz (Video S2). For the temperature sensor, it can also be driven by CPV-TENG. And before the temperature sensor can work, a commercial capacitor of 33 μF must arrive at the voltage of 1.5 V (Fig. 5 f). Furthermore, the temperature sensor can also effectively work under a wideband frequency range from 18 to 38 Hz (Video S3). Considering the high output under a wideband frequency range of the CPV-TENG, some different sensors can be developed and applied for industrial equipment warning and the Internet of Things.

Supplementary material related to this article can be found online at doi:10.1016/j.nanoen.2022.107427.

3. Conclusions

In summary, the frequency band broadening mechanism and charge density enhancement technique of the V-TENG with two stoppers were elaborated in detail. The introduction of double-sided stoppers strengthens the nonlinear features and broadens the frequency range of the V-TENG. Based on the dual-channel output of the V-TENG, a charge pump can be designed to enhance the charge density. Therefore, based on the single-degree-of-freedom model of the V-TENG with two stoppers, the frequency band broadening mechanism and the law of influence of parameters were expounded detailed by the way of simulation analysis and experimental verification. Meanwhile, the V-TENG based on two stoppers and a single stopper was compared and analyzed. As a result, the broad frequency band characteristics of the V-TENG would become more obvious with the optimized distance and excitation acceleration as well as the V-TENG with two stoppers has a wider working bandwidth than with one stopper. And the frequency band of the V-TENG with two stoppers would be 75% broadener than one stopper under the gap distance of 0.5 mm. Furthermore, a high-performance CPV-TENG is constructed, which can obtain a high surface charge density and has improved by about 14 times. With the frequency changes from 18 to 38 Hz, the CPV-TENG can continually power 400 LEDs and charge a commercial capacitor quickly. In the same frequency band, the CPV-TENG can quickly drive a temperature sensor and a pressure sensor to work. Since the CPV-TENG can obtain a high output performance under a wide frequency range, it can effectively obtain wideband vibration energy from machines, cars, ships, and human motions.

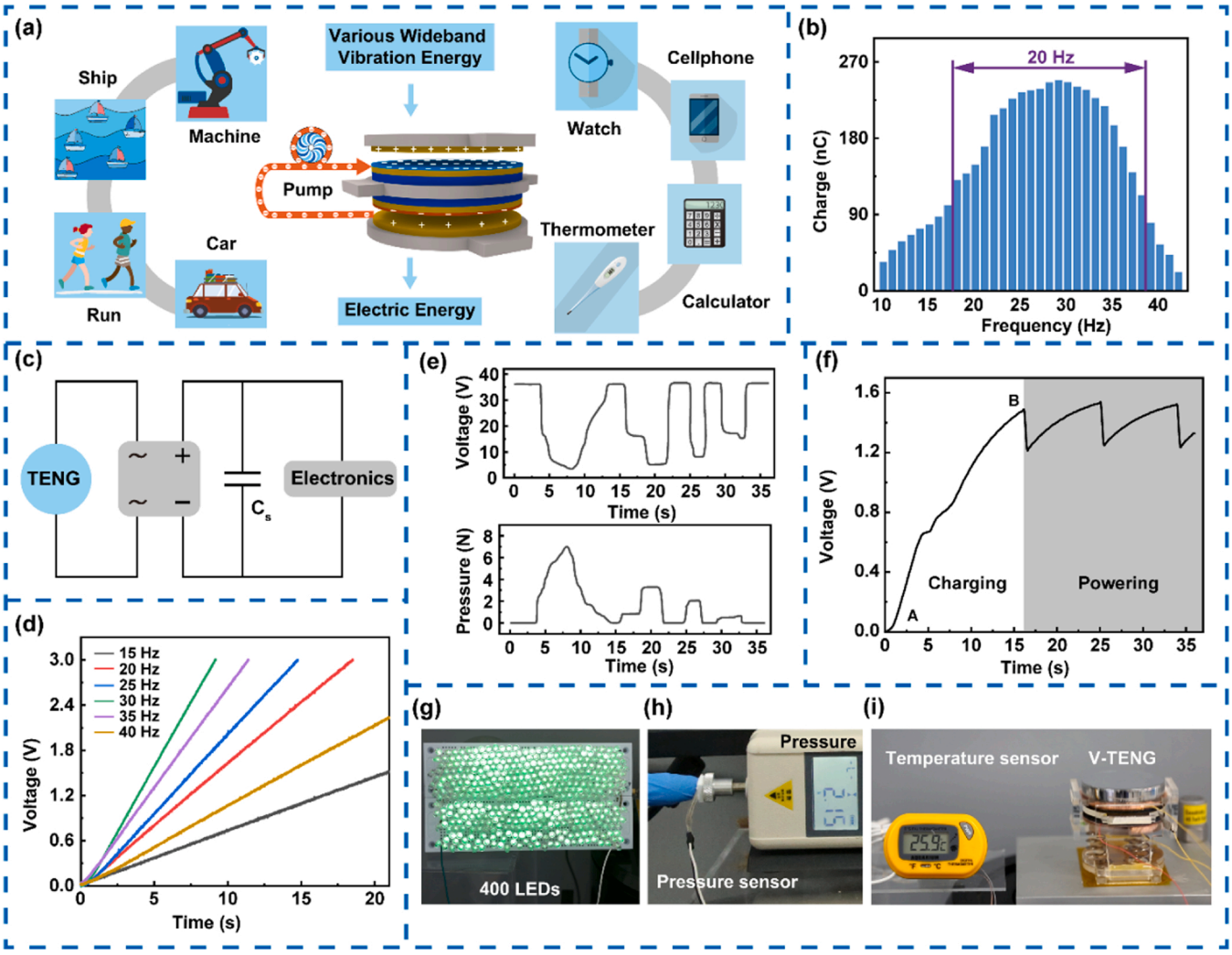

Fig. 5. Performance characterization and potential application of the CPV-TENG. (a) CPV-TENG to harvest vibrational energy for powering various electronic devices. (b) Charge response of the CPV-TENG under wideband change of frequencies. (c) Circuit diagram of the CPV-TENG for powering electronics. (d) Voltage change curve of a 33 μF capacitor under broadband vibration conditions with the excitation acceleration of 6 m/s^2. Voltage charging curves of the CPV-TENG for powering a Pressure sensor (e) and Temperature sensor (f). (g-i) Photographs of the V-TENG powering 400 light-emitting diodes (g), a Pressure sensor (h), and a Temperature sensor (i).

4. Method

4.1. Fabrication of the V-TENG

Firstly, a laser fast scanning and cutting machine (D90M) was used to cut many acrylic sheets with a radius of 24 mm. After that, an acrylic sheet was chosen as support and distributed the three springs (25 mm in height, 12 mm in diameter) evenly on it. Then, two acrylic sheets were chosen as moving parts and stuck a copper film (48 mm in diameter, 65 μm in thickness) on one side as the friction layer. Another acrylic sheet was selected as the fixed part. And attached sponge (48 mm in diameter, 3 mm in thickness) and PTFE (48 mm in diameter, 80 μm in thickness) on one side in turn, and attached sponge and Kapton (48 mm in diameter, 6 μm in thickness) on the other side. Furthermore, the two sides of the fixed part were also considered as two stoppers. Then, placed these acrylic sheets in sequence according to the model diagram shown in Fig. 1a. And the two moving parts were connected with the connecting plate, and the fixed part and the base were also connected with the connecting plate. Leading out the two electrodes with wires for electrical measurement.

4.2. Electric measurements

The field emission scanning electron microscope (Quanta 450) is selected as characterization equipment to characterize the surface micro-nano structures of the PTFE film. The electrometer (Keithley 6514 system electrometer) was used to characterize the charge, current, and voltage of the V-TENG. Therein, the electrical output can be measured by both the grounding method and the non-grounding measuring method [37,38]. What's more, the electrostatic voltmeter (Trek 347) was used to measure the large voltage of the CPV-TENG. Mechanical vibration was simulated by a vibration shaker (KSI-758ST500) equipped with vibrational control equipment (VT-9002) and power amplifier equipment (KSI-758PA800). And the laser ranging instrument (HL-G103-A-C5) is chosen as the characterization equipment to measure the amplitude of the V-TENG. Furthermore, the real-time data was recorded by a software platform developed based on LabVIEW.

CRediT authorship contribution statement

Youchao Qi, GuoXu Liu, and Yang Kuang contributed equally. Youchao Qi, GuoXu Liu, Yang Kuang, Meiling Zhu, and Chi Zhang conceived the idea and put forward experimental methods. Youchao Qi, Lu Wang,

Jianhua Zeng, Yuan Lin, and Han Zhou built a test platform and visualized it. Youchao Qi, Guoxu Liu, and Yang Kuang did the experiments and wrote the research paper. Youchao Qi and Guoxu Liu processed the data of the experiment. Youchao Qi, Lu Wang, and Yang Kuang designed corresponding Figures. Meiling Zhu and Chi Zhang directed this project.

Declaration of Competing Interest

The authors declare that they have no known competing financial interests or personal relationships that could have appeared to influence the work reported in this paper.

Acknowledgments

This research was supported by the National Natural Science Foundation of China (Nos. 51922023, 61874011), and Fundamental Research Funds for the Central Universities (E1EG6804).

Appendix A. Supporting information

Supplementary data associated with this article can be found in the online version at doi:10.1016/j.nanoen.2022.107427.

References

[1] M. Pundir, J.K. Sandhu, A systematic review of quality of service in wireless sensor networks using machine learning: recent trend and future vision, J. Netw. Comput. Appl. 188 (2021), 103084.
[2] S. Umamaheswari, Hybrid optimization model for energy efficient cloud assisted wireless sensor network, Wirel. Pers. Commun. 118 (2021) 873–885.
[3] S. Wang, L. Lin, Y. Xie, Q. Jing, S. Niu, Z.L. Wang, Sliding-triboelectric nanogenerators based on in-plane charge-separation mechanism, Nano Lett. 13 (2013) 2226–2233.
[4] H. Qin, G. Cheng, Y. Zi, G. Gu, B. Zhang, W. Shang, F. Yang, J. Yang, Z. Du, Z. L. Wang, High energy storage efficiency triboelectric nanogenerators with unidirectional switches and passive power management circuits, Adv. Funct. Mater. 28 (2018), 1805216.
[5] W. Shang, G. Gu, W. Zhang, H. Luo, T. Wang, B. Zhang, J. Guo, P. Cui, F. Yang, G. Cheng, Z. Du, Rotational pulsed triboelectric nanogenerators integrated with synchronously triggered mechanical switches for high efficiency self-powered systems, Nano Energy 82 (2021), 105725.
[6] J. He, X. Fan, D. Zhao, M. Cui, B. Han, X. Hou, X. Chou, A high-efficient triboelectric-electromagnetic hybrid nanogenerator for vibration energy harvesting and wireless monitoring, Sci. China-Inf. Sci. 65 (2021), 142401.
[7] X. Wang, S. Niu, F. Yi, Y. Yin, C. Hao, K. Dai, Y. Zhang, Z. You, Z.L. Wang, Harvesting ambient vibration energy over a wide frequency range for self-powered electronics, ACS Nano 11 (2017) 1728–1735.
[8] K. Fan, G. Liang, D. Wei, W. Wang, S. Zhou, L. Tang, Achieving high-speed rotations with a semi-flexible rotor driven by ultralow-frequency vibrations, Appl. Phys. Lett. 117 (2020), 223901.
[9] U. Erturun, A. Eisape, J.E. West, Design and analysis of a vibration energy harvester using push-pull electrostatic conversion, Smart Mater. Struct. 29 (2020), 105018.
[10] L. Tang, Y. Yang, C.K. Soh, Toward broadband vibration-based energy harvesting, J. Intell. Mater. Syst. Struct. 21 (2010) 1867–1897.
[11] J. Kim, A study on the analytic power estimation of the electromagnetic resonant energy harvester for the high-speed train, Electronics 9 (2020) 403.
[12] Y. Fu, M. Huang, R. Wu, F. Huang, M. Zhou, S. Chen, Q. Wang, Q. Li, Piezoelectric vibration energy harvesting device based on water sloshing-inspired extensions, AIP Adv. 11 (2021), 065205.
[13] H. Liu, C. Lee, T. Kobayashi, C.J. Tay, C. Quan, Investigation of a MEMS piezoelectric energy harvester system with a frequency-widened-bandwidth mechanism introduced by mechanical stoppers, Smart Mater. Struct. 21 (2012), 035005.
[14] Z.C. Ong, Y.X. Ooi, S.Y. Khoo, Y.H. Huang, Two-stage multi-modal system for low frequency and wide bandwidth vibration energy harvesting, Measurement 149 (2020), 106981.
[15] I. Abed, N. Kacem, N. Bouhaddi, M.L. Bouazizi, Multi-modal vibration energy harvesting approach based on nonlinear oscillator arrays under magnetic levitation, Smart Mater. Struct. 25 (2016), 025018.
[16] Y. Qin, S. Wang, T. Wei, R. Chen, A wide band nonlinear dual piezoelectric cantilever energy harvester coupled by origami, Smart Mater. Struct. 30 (2021), 025025.
[17] D. Wang, Z. Hao, F. Chen, Y. Chen, Nonlinear energy harvesting with dual resonant zones based on rotating system, Appl. Math. Mech. 42 (2021) 275–290.
[18] D. Zou, G. Liu, Z. Rao, T. Tan, W. Zhang, W.-H. Liao, A device capable of customizing nonlinear forces for vibration energy harvesting, vibration isolation, and nonlinear energy sink, Mech. Syst. Signal Proc. 147 (2021), 107101.
[19] F.-R. Fan, Z.-Q. Tian, Z.L. Wang, Flexible triboelectric generator, Nano Energy 1 (2012) 328–334.
[20] T. Wang, G. Gu, W. Shang, J. Gan, W. Zhang, H. Luo, B. Zhang, P. Cui, J. Guo, F. Yang, G. Cheng, Z. Du, A self-powered photodetector using a pulsed triboelectric nanogenerator for actual working environments with random mechanical stimuli, Nano Energy 90 (2021), 106518.
[21] J. Zhao, G. Zhen, G. Liu, T. Bu, W. Liu, X. Fu, P. Zhang, C. Zhang, Z.L. Wang, Remarkable merits of triboelectric nanogenerator than electromagnetic generator for harvesting small-amplitude mechanical energy, Nano Energy 61 (2019) 111–118.
[22] X. Pu, M. Liu, L. Li, S. Han, X. Li, C. Jiang, C. Du, J. Luo, W. Hu, Z.L. Wang, Wearable textile-based in-plane microsupercapacitors, Adv. Energy Mater. 6 (2016), 1601254.
[23] W. Tang, T. Jiang, F.R. Fan, A.F. Yu, C. Zhang, X. Cao, Z.L. Wang, Liquid-metal electrode for high-performance triboelectric nanogenerator at an instantaneous energy conversion efficiency of 70.6%, Adv. Funct. Mater. 25 (2015) 3718–3725.
[24] X. Liu, P. Cui, J. Wang, W. Shang, S. Zhang, J. Guo, G. Gu, B. Zhang, G. Cheng, Z. Du, A robust all-inorganic hybrid energy harvester for synergistic energy collection from sunlight and raindrops, Nanotechnology 32 (2020), 075401.
[25] J. Chun, B.U. Ye, J.W. Lee, D. Choi, C.-Y. Kang, S.-W. Kim, Z.L. Wang, J.M. Baik, Boosted output performance of triboelectric nanogenerator via electric double layer effect, Nat. Commun. 7 (2016) 12985.
[26] S. Zhang, J. Guo, L. Liu, H. Ruan, C. Kong, X. Yuan, B. Zhang, G. Gu, P. Cui, G. Cheng, Z. Du, The self-powered artificial synapse mechanotactile sensing system by integrating triboelectric plasma and gas-ionic-gated graphene transistor, Nano Energy 91 (2022), 106660.
[27] F. Xu, S. Dong, G. Liu, C. Pan, Z.H. Guo, W. Guo, L. Li, Y. Liu, C. Zhang, X. Pu, Z. L. Wang, Scalable fabrication of stretchable and washable textile triboelectric nanogenerators as constant power sources for wearable electronics, Nano Energy 88 (2021), 106247.
[28] Z.L. Wang, A.C. Wang, On the origin of contact-electrification, Mater. Today 30 (2019) 34–51.
[29] J. Chen, Z.L. Wang, Reviving vibration energy harvesting and self-powered sensing by a triboelectric nanogenerator, Joule 1 (2017) 480–521.
[30] Y. Qi, G. Liu, Y. Gao, T. Bu, X. Zhang, C. Xu, Y. Lin, C. Zhang, Frequency band characteristics of a triboelectric nanogenerator and ultra-wide-band vibrational energy harvesting, ACS Appl. Mater. Interfaces 13 (2021) 26084–26092.
[31] D. Bhatia, W. Kim, S. Lee, S.W. Kim, D. Choi, Tandem triboelectric nanogenerators for optimally scavenging mechanical energy with broadband vibration frequencies, Nano Energy 33 (2017) 515–521.
[32] W. Sun, Z. Jiang, X. Xu, Q. Han, F. Chu, Electromechanical coupling modeling and analysis of contact-separation mode triboelectric nanogenerators, Int. J. Non-Linear Mech. 136 (2021), 103773.
[33] Y. Zi, S. Niu, J. Wang, Z. Wen, W. Tang, Z.L. Wang, Standards and Fig.-of-merits for quantifying the performance of triboelectric nanogenerators, Nat. Commun. 6 (2015) 8376.
[34] T. Zhou, L. Zhang, F. Xue, W. Tang, C. Zhang, Z.L. Wang, Multilayered electret films based triboelectric nanogenerator, Nano Res 9 (2016) 1442–1451.
[35] J. Wang, C. Wu, Y. Dai, Z. Zhao, A. Wang, T. Zhang, Z.L. Wang, Achieving ultrahigh triboelectric charge density for efficient energy harvesting, Nat. Commun. 8 (2017) 88.
[36] H. Wang, L. Xu, Y. Bai, Z.L. Wang, Pumping up the charge density of a triboelectric nanogenerator by charge-shuttling, Nat. Commun. 11 (2020) 4203.
[37] W. Zhang, G. Gu, H. Qin, S. Li, W. Shang, T. Wang, B. Zhang, P. Cui, J. Guo, F. Yang, G. Cheng, Z. Du, Measuring the actual voltage of a triboelectric nanogenerator using the non-grounded method, Nano Energy 77 (2020), 105108.
[38] W. Zhang, G. Gu, W. Shang, H. Luo, T. Wang, B. Zhang, P. Cui, J. Guo, F. Yang, G. Cheng, Z. Du, A general charge compensation strategy for calibrating the voltage of a triboelectric nanogenerator measured by a capacitive circuit, Nano Energy 86 (2021), 106056.

Youchao Qi received his B.E. degree in Mechanical Engineering and Automation from Yantai University in 2018. He is currently pursuing his Ph.D degree in the Beijing Institute of Nano energy and Nano systems, Chinese Academy of Sciences. His research interests mainly focus on triboelectric nanogenerator for vibration energy harvesting.

Guoxu Liu received his Ph.D degree in Condensed matter physics from National center for Nanoscience and technology in 2021. Now he is a Post-doctorate at Shenzhen University and visiting scholar at Beijing Institute of Nanoenergy and Nanosystems, Chinese Academic Science. His current research mainly focuses on 3D printing triboelectric based wearable energy harvesting device.

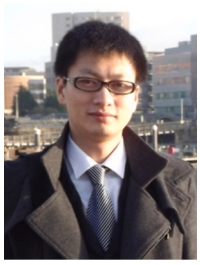

Yang Kuang received his B.Eng. and M.Eng. from Central South University and PhD in Mechanical Engineering from the University of Dundee. Since then, he has been working at the University of Exeter, initially as an associate research fellow and later as a research fellow. His main research is focused on self-powered wireless sensing systems enabled by energy harvesting.

Lu Wang received the B.S. degree of Mechanical Engineering and Automation in July 2013 and Ph.D. degree in 2021, both in Xi'an Jiaotong University, and one year exchange as visiting Ph.D in National University of Singapore. His research interests include energy harvesting, MEMS sensors and actuator, and structural vibration.

Jianhua Zeng received his master degree in School of Mechanical and Electrical Engineering from Guilin University of Electronic Technology in 2018. Now he is currently studying for the Ph.D candidate in the School of Physical Science and Technology, Guangxi University, China. His research interests mainly focus on tribotronics and intelligent devices.

Yuan Lin received his bachelor's degree from Changchun University of Science and Technology in 2012. Now he is a master degree candidate in School of Mechanical Engineering, Guangxi University, China. His research interests mainly focus on tribotronics and intelligent devices.

Han Zhou received his bachelor degree in College of Mechanical Engineering and Automation from Huaqiao University in 2019. He is currently pursuing a master's degree in the School of Mechanical Engineering, Guangxi University, China. His research interests mainly focus on power management for TENG and self-powered systems.

Meiling Zhu received the B.Eng., M.Eng., and Ph.D. degrees from Southeast University, Nanjing, China, in 1989, 1992, and 1995, respectively. She is currently a Professor and the Chair of Mechanical Engineering and the Head of the Energy Harvesting Research Group with the University of Exeter, U.K. Her current research is concentrated on energy harvesting powered wireless communication and sensor nodes.

Chi Zhang received his Ph.D. degree from Tsinghua University in 2009. After graduation, he worked at Tsinghua University as a postdoc research fellow and NSK Ltd., Japan as a visiting scholar. He now is the principal investigator of Tribotronics Group in Beijing Institute of Nanoenergy and Nanosystems, Chinese Academy of Sciences (CAS), Member of Youth Innovation Promotion Association, CAS. Prof. Chi Zhang's research interests are triboelectric nanogenerator, tribotronics, self-powered MEMS/NEMS, and applications in flexible electronics, intelligent equipment and the Internet of things.